Pulse-train control of branching processes: Elimination of background- and intruder state population

Markus Seidl,[1] Mihajlo Etinski,[2*] Christoph Uiberacker,[1†] and Werner Jakubetz [1‡]

[1] *Department of Theoretical Chemistry, University of Vienna, Währinger Str. 17, 1090 Wien, Austria*

[2] *Faculty of Physical Chemistry, University of Belgrade, Studentski trg 12-16, 11000 Beograd, Serbia*

[*] Present address: Institute of Theoretical and Computational Chemistry, Heinrich Heine University Düsseldorf, 40225 Düsseldorf, Germany

[†] Present address: Institute for Physics, University of Leoben, 8700 Leoben, Austria

[‡] Electronic mail: werner.jakubetz@univie.ac.at

ABSTRACT

The authors introduce and describe pulse train control (PTC) of population branching in strongly coupled processes as a novel control tool for the separation of competing multiphoton processes. Control strategies are presented based on the different responses of processes with different photonicities and/or different frequency detunings to the pulse-to-pulse time delay and the pulse-to-pulse phase shift in pulse trains. The control efficiency is further enhanced by the property of pulse trains that complete population transfer can be obtained over an extended frequency range that replaces the resonance frequency of simple pulses. The possibility to freely tune the frequency assists the separation of the competing processes and reduces the number of sub-pulses required for full control. As a sample application, PTC of leaking multiphoton resonances is demonstrated by numerical simulations. In model systems exhibiting sizable background- (intruder-) state population if excited with single pulses, PTC leading to complete accumulation of population in the target state and elimination of background population is readily achieved. The analysis of the results reveals different mechanisms of control and provides clues on the mechanisms of the leaking process itself. In an alternative setup, pulse trains can be used as a phase-sensitive tool for level switching. By changing only the pulse-to-pulse phase shift of a train with otherwise unchanged parameters, population can be transferred to any of two different target states in a near-quantitative manner.

1. INTRODUCTION

Recently, three of us[1] have explored the conditions under which simple π-pulses [2,3] (more precisely, generalized π-pulses [4]) governing multiphoton (mp) transitions along anharmonic progressions can be replaced by trains of fractional π-pulses. In particular, we characterized fitness landscapes for train-induced population transfer, and demonstrated that there exist extended regions in parameter space, denoted "resonance loci", which are associated with pulse trains effecting complete state-specific population transfer ("π-trains"). The control properties are sensitive to variations of the pulse-to-pulse (ptp) time delays and ptp phase shifts, as well as to the obvious parameters frequency and field strength, such that the projection of the resonance loci onto the frequency-field strength plane produces closed curves ("resonance ridges"). As an important consequence, as first pointed out by Vitanov and Knight,[5] an extended frequency range is available for complete population transfer, where specific resonance field strengths are associated which each frequency value in the range spanned by the resonance ridges.[1]

In conjunction with earlier papers on pulse-train induced population transfer,[5-9] the results of ref. 1 provide a starting point for pulse train control (PTC) of parallel or branching processes. If such processes involve near-degenerate transition frequencies and/or different photonicities, they should be separable due to their different responses to the ptp time delays and ptp phase shifts. Furthermore, control should be facilitated by the option to freely tune the frequency without loss of transfer efficiency, and also to "tune" the number of sub-pulses. With these properties, PTC based on phase-matching and phase-recurrence properties is a novel tool for the control of competing mp population transfer processes, *e.g.* competing reaction channels. Pulse trains ("multipulses") with properties as required in the present application have become available in the laboratory [7,10,11] Very recently, they have been applied for control purposes in population transfer by adiabatic passage [10] and state-specific vibronic excitation.[11]

A scenario for an application of the control properties of pulse trains is PTC of leaking resonances.[12-14] Resonance leaking occurs if in a transition driven by a π-pulse or multiple-order π-pulse population is diverted ("leaks") to an intruder state. Even very weakly coupled states (background states) may act as efficient intruders quenching the primary transition strongly or completely, and if the coupling to a background state occurs in Λ-configuration, leaking can be a robust phenomenon.[13] As such a situation involves near-degenerate processes of different photonicities, it naturally addresses the dominant aspects of PTC and thus provides a suitable testing ground for our proposed control strategies. While the control of leaking resonances by *pairs* of optimized phase-adjusted pulses has been discussed before,[13,14] pulse trains offer a considerably higher degree of flexibility. Even tuning a single train parameter may suffice to achieve far-reaching control, at least in cases where zero-order relations based on the rotating-wave approximation (RWA) [2,3] hold. However, in more complex situations restrictions will apply which dictate how closely the idealized limits may be approached under realistic conditions.

In the present paper, by numerical simulations on model systems we demonstrate PTC of background- (or intruder-) state population. In Section 2 we summarize the properties of our model systems consisting of Morse progressions augmented by a weakly bound background level. The systems are designed to exhibit considerable resonance leaking if driven with simple (gaussian) pulses in the low picosecond range, thus quenching the targeted mp transition and producing massive population transfer to the background state. In Section 3 we describe the pulse trains used, and elaborating from the results for population transfer in anharmonic progressions in ref. 1, we suggest specific PTC strategies for the elimination of intruder state population. Section 4, arranged in several subsections, contains the results of our simulations together with a discussion. We show that resonance leaking in a two-photon transition can be readily controlled starting from zero-order estimates. PTC of a five-photon transition is also

readily achieved, but requires more extended parameter optimization. We identify different mechanisms of PTC and show how this can reveal different mechanisms of resonance leaking. In Sec. 5 we describe a variant of PTC set up as tool for phase-controlled level switching. Finally, in Section 6 we summarize the advantages and limitations of PTC and its application to other forms of population branching.

2. MODEL SYSTEMS

Our model systems are constructed from anharmonic progressions, augmented with a background state weakly coupled to the anharmonic ladder. The pure ladder systems and their behavior under resonant mp excitation by pulse trains have been investigated in ref. 1; we use these results as reference for the present study.

In the augmented systems we study *n*-photon excitation along the anharmonic ladder from an *initial* state $|\mathrm{I}\rangle$ to a *final* (or target) state $|\mathrm{F}\rangle$. The $N = n + 1$ ladder states are also labeled $|1\rangle$ to $|N\rangle$, and connecting to previous work on resonance leaking,[13,14] the level energies ε_1 to ε_N are given by Morse states adapted from the HCN bend progression. In each system the rung spacing ($\varepsilon_N - \varepsilon_{N-1}$) is set to 0.00425 a.u., and consecutively lower level spacings are incremented by 0.00025 a.u. To these ladder systems we add a *background* (or intruder) state $|\mathrm{B}\rangle$ weakly coupled to $|\mathrm{F}\rangle$, either in Λ-configuration with level energy $\varepsilon_\mathrm{B} < \varepsilon_\mathrm{F}$, so that $|\mathrm{F}\rangle$ becomes the apex of an extended Λ-system, or in ladder-configuration with $\varepsilon_\mathrm{B} > \varepsilon_\mathrm{F}$.

In the context of PTC, an important difference between the ladder and extended-Λ configurations is the fact that in the former the overall photonicity for the $|\mathrm{I}\rangle \rightarrow |\mathrm{B}\rangle$ excitation is $n-1$, while in the latter $|\mathrm{B}\rangle$ is reached in a process of overall photonicity $n+1$.

For each of the augmented systems, ε_{B} is adjusted such that appreciable resonance leaking occurs for gaussian pulses with durations of few picoseconds. In such a case the zero-order resonance frequency of the *n*-photon transition $|\mathrm{I}\rangle \rightarrow |\mathrm{F}\rangle$ along the ladder,

$$\omega_0^{\mathrm{IF}} = (\varepsilon_{\mathrm{F}} - \varepsilon_{\mathrm{I}})/n\hbar\,, \tag{1}$$

and the 1-photon $|\mathrm{F}\rangle \rightarrow |\mathrm{B}\rangle$ transition frequency

$$\omega_0^{\mathrm{FB}} = |\varepsilon_{\mathrm{F}} - \varepsilon_{\mathrm{B}}|/\hbar \tag{2}$$

are near-degenerate [14] – *not* strictly degenerate due to their different Bloch-Siegert shifts.[16] The values of ω_0^{FB} used in our model systems are given in Table I. We note that for a pulse or pulse train at central frequency $\omega_{\mathrm{r}}^{\mathrm{IF}}$ the individual levels $|i\rangle$ of the anharmonic ladder are characterized by their rung detuning $d\varepsilon_i$,

$$d\varepsilon_i = |(\varepsilon_i - \varepsilon_1) - i\,\omega_{\mathrm{r}}^{\mathrm{IF}}|\,. \tag{3}$$

All systems are assumed to be non-polar, and to be sequentially coupled, with dipole matrix elements $\mu_{ij} = \mu_{\mathrm{L}} = 0.2$ a.u.; these values are again adapted from the HCN bend progression.[17] As in previous investigations,[13,14] $|\mathrm{B}\rangle$ is assumed to be weakly coupled to $|\mathrm{F}\rangle$, with dipole matrix element $\mu_{\mathrm{FB}} = 0.02$ a.u.

In the present paper we focus on three model systems illustrated in Fig. 1. With $N = 6$, the system denoted "(6+1)ΛS" is an extended Λ-system, so that $|\mathrm{B}\rangle$ is energetically near-degenerate with rung state $|5\rangle$. The nominal 6-level systems denoted "embedded (3+1)ΛS" and "embedded (3+1)LS" are derived from standard (3+1)-level systems and are used to study PTC of resonance leaking for a 2-photon transition. In order to explore the consequences of embedding the ladder states into a longer anharmonic progression,[1] we add one level below $|\mathrm{I}\rangle$, denoted $|-\rangle$, and one level above $|\mathrm{F}\rangle$, denoted $|+\rangle$. Hence $|\mathrm{B}\rangle$ is energetically near-

degenerate with rung state $|2\rangle$ in the embedded (3+1)ΛS, and near-degenerate with the outer rung state $|+\rangle$ in the embedded (3+1)LS. In the vast majority of simulations reported here, the results for the systems with and without the embedding extension are almost indistinguishable. Therefore we will not continue to make the distinction and drop the term "embedded".

We have also investigated systems with 4 and 5 ladder states, but we will gloss only briefly over the corresponding results, which do not provide additional insight into PTC.

Pulse parameters for resonant, but leaking mp excitation by gaussian pulses with pulse length $T_{\rm p} = 8$ ps, measured as full-width at half-height (fwhh) in field strength, are collected in Table II, together with corresponding data for population branching. Results for π-train excitation in the simple anharmonic ladders have been given in ref. 1.

3. PULSE TRAIN CONTROL OF INTRUDER STATE POPULATION

3.1. Pulse trains

We employ pulse trains in a setup that we have previously denoted *m*-trains.[1] Such *m*-trains consist of *m* equal gaussian (sub-) pulses of frequency ω, gaussian amplitude A_0 and length T_m (again measured as fwhh in field strength), with equal ptp phase shifts $\delta_{\rm ptp}$ and ptp time delays $\Delta_{\rm ptp}$, the latter limited from below by the requirement that the sub-pulses be effectively non-overlapping. We keep $T_m = T_{\rm p}/m$, thus focusing on the problem to split a single (resonant) π-pulse into fractional π-pulses, such that the parameters ω, A_0, $\delta_{\rm ptp}$ and $\Delta_{\rm ptp}$, and also *m*, can be tuned to control specific processes. In this setup the total fluence of the π-train is (approximately) equal to that of the π-pulse for any mp process driven.

Another limiting setup for equal fractional π-pulses would be to keep the sub-pulse width at $T_m = T_{\rm p}$ and to reduce the field strength accordingly. Giving rise both to extended overall

train duration and increased total fluence, this strategy is of little relevance in the control of resonance leaking, although it may be an option in applications where strong fields must be avoided. A sketch of both setups is shown in Fig. 2.

3.2. Implications from the background-free systems

In an RWA-related zero-order picture a *k*-photon transition along an anharmonic ladder can be driven *on resonance* ($\omega = \omega_0^k$) with a suitable π-pulse, or equivalently[1] with π-trains, *i.e. m*-trains of arbitrary Δ_{ptp} with δ_{ptp} chosen as

$$\delta_{\mathrm{ptp}} = \nu 2\pi / k\,, \quad \nu \text{ integer}, \tag{4}$$

while the transition is quenched if ν in eq. (4) is taken half-integer.

Assume now that in a system incorporating such a ladder a targeted *k*-photon transition $|\mathrm{I}\rangle \rightarrow |\mathrm{F}\rangle$ is perturbed by a second process $|\mathrm{I}\rangle \rightarrow |\mathrm{B}\rangle$ of different photonicity *l*, with almost or even exactly the same resonance parameters ($A_r^l, \omega_{\mathrm{r}}^l$), and, for simplicity, $\omega_0^l = \omega_0^k$, so that both processes are driven by the original π-pulse and are subject to competition, interaction and interference. It should then be possible to separate the two processes on the basis of *m*-trains with suitably chosen phase relations. The *k*-photon process would run selectively with any ptp phase shift $\delta_{\mathrm{ptp}} = \nu 2\pi / k$ that is not also element of $\{\nu 2\pi / l\}$, and vice versa for the *l*-photon process. Since $k \neq l$ is assumed, such choices are always possible except for $l = 2k, 3k, \ldots$, when only the process of higher photonicity may be separated. Dropping zero-order assumptions, this simple picture has to be modified. Depending on the system and the remaining train parameters, appropriate values of δ_{ptp} deviate from the estimates in eq. (4).[1]

Since with pulse trains complete (resonant) population transfer can be maintained over a range of frequencies,[1,5] separation of two processes with *near-degenerate* zero-order resonance

frequencies $\omega_0^l \neq \omega_0^k$ by *m*-trains may be achieved by tuning to a suitable ω and adjusting Δ_{ptp} and/or δ_{ptp}. Thus at frequency ω and fixed δ_{ptp}, for any *k*-photon process constructive interference accumulating population in the target state recurs with phase recurrence time T_δ,

$$T_\delta = \frac{2\pi}{k\left|\omega - \omega_0^k\right|}. \tag{5}$$

This gives rise to oscillatory target populations as a function of Δ_{ptp}; the pattern may be irregular due to contributions from other states. The different phase recurrence times of two non-degenerate processes enable control of their branching by optimization of Δ_{ptp} and δ_{ptp} such that the two processes are in turn subject to constructive and destructive interference. This behavior is simplified if the frequency is set to $\omega = \omega_0^k$ or to $\omega = \omega_0^l$ (see items A and B in Sec. 3.3).

The availability of free frequency variation along extended resonance ridges is a strong asset in the separation of branching transitions, which due to their different photonicities will respond differently to frequency tuning.

The results in ref. 1 also indicate the role of *m* as an adjustable parameter. As the number of sub-pulses increases, the frequency range available for resonant excitation increases, and the interference peaks that give rise to accumulation of population become narrower with respect to δ_{ptp} and Δ_{ptp}. Both effects assist the separation of competing population transfer processes. Conversely, it also means reduced robustness, and in particular it is clear that a switch to "*m*-regime II" (the regime of many sub-pulses [1]) with its manifest rung population will make PTC a much more complex exercise.

3.3. Strategies for the elimination of intruder state population

We start by considering leaking as a simple perturbation, such that control of the target state population in the presence of the intruder is as in the simple background-free anharmonic NLSs. Among the set of $(n)\pi$-trains occupying the resonance loci of the background-free system, we have to identify those that suppress intruder state population. In real systems we must expect that the presence of the intruder state will modify the π-train parameters, and hence readjustment of these parameters will be required. These changes may be weak for a truly leaking resonance, or sizable if the intruder transition imprints its properties onto the overall process (see ref. 11 and Sec. 4.3 for a discussion of different leaking mechanisms).

Together with conclusions from Section 3.2, these considerations suggest the following specific PTC strategies:

A. *Tuning to* ω_0^{IF}. Due to $T_\delta \to \infty$ in eq. (5), P_{F} will be enhanced independent of Δ_{ptp} for any of the constructive values of δ_{ptp}; suitable zero-order estimates are given by eq. (4), and δ_{ptp} drops out of the optimization. With the resonance value of A_0, Δ_{ptp} must be adjusted to minimize intruder- *and* rung populations. This can be achieved because of the different phase recurrence times of the different levels.

B. *Tuning to* ω_0^{IB}. A situation comparable to method A occurs for $\omega = \omega_0^{\mathrm{IB}}$, whence intruder population will be suppressed independent of Δ_{ptp} by the choice of a value of δ_{ptp} destructive for the $|\mathrm{I}\rangle \to |\mathrm{B}\rangle$ transition.

C. *Free frequency tuning*. As noted above, variation of ω will assist the separation of branching transitions and should allow efficient solutions in the sense that the number of sub-pulses can be minimized.

Methods A and B carry elements of *a priori* planning, and useful results may be obtained from zero-order estimates used either directly or as startup values. For method C there are no *a priori* hints other than from simulations; in theoretical work initial conditions for optimization could be obtained from the resonance ridges of the background-free systems.

In all three cases we should also expect that the regular behavior of pulse train excitation in anharmonic progressions will be modified by interference contributions from the intruder, constructively or destructively. Exploiting such multiple specific interferences, there may also be solutions without counterpart in the background-free system, *i.e*., away from the resonance ridges of the simple systems, that are not based on the systematic properties of PTC. Such "irregular" solutions can be seen as cases of general pulse-shaping and are best obtained by (constrained) optimal control,[18] most efficiently by self-learning algorithms.[19,20]

4. RESULTS FOR PULSE-TRAIN-CONTROL OF RESONANCE LEAKING

4.1. Overview

An overview of the performance of PTC in the suppression of resonance leaking is given in Fig. 3 and 4, where we compare the population dynamics for resonant, but leaking gaussian π-pulses (with parameters shown in Table II) for the (3+1)ΛS and the (6+1)ΛS, respectively, with those for suitably optimized *m*-trains. We note that results for the (4+1)ΛS and (5+1)ΛS are in close qualitative agreement with those for the (6+1)ΛS. While 8 ps gaussian pulses designed to pump the $|\mathrm{I}\rangle \rightarrow |\mathrm{F}\rangle$ transitions induce strong background leaking, it is seen that for equivalent π-trains P_F reaches or exceeds 0.99. The examples cover various control strategies introduced above including also multiple-π trains and are "efficient" implementations of the PTC strategies suggested in Sec. 3.3 in the sense of keeping the number of sub-pulses low and the train duration as short as possible.

In the (3+1)ΛS, all PTC fields shown can be classified as regular solution closely resembling π-trains for corresponding 3LS. With methods A and B, at least 6-trains as shown in Fig. 3b and c are required to meet the control criterion $P_F > 0.99$. Detuning ω is a very efficient strategy that can produce fully selective 4-trains (Fig. 3d).

More irregular behavior is displayed by the solutions for the (6+1)ΛS, most auspiciously by the 4-train solution. Here the population dynamics retains none of the characteristics of pulse train excitation in the background-free system. It obviously belongs to the irregular solutions anticipated above.

In the following subsections we will discuss the properties of the types of solutions of the control problem, and will work out the systematic features in the behavior of PTC and the relation to simple pulse train excitation in the corresponding background-free systems.

4.2. Resonance ridges, regular and irregular solutions

In the background-free systems, the multiple points in parameter space denoting π-trains due to their phase recurrence properties can be projected on resonance ridges in the (ω, A_0)-plane. As a working assumption, with the intruder fully suppressed a π-train in an augmented system might resemble that in the background-free ladder system. In Fig. 5a we compare resonance ridges for 4-trains driving the 3LS [1] with corresponding PTC results for (3+1)ΛS. Indeed we observe only weak changes in the train amplitudes, and negligible ones in the frequency range covered. Furthermore the profiles along cuts at fixed ω, shown in Fig 5b and c, are very close. In the presence of the intruder state the resonance ridge is thus retained as projection of the loci of *at least approximate* π-trains. The qualification is made because the points shown for the (3+1)ΛS do not consistently match the criterion $P_F > 0.99$. They do near

the coalescence points, *e.g.* along the cut marked "c". The population dynamics for the corresponding control field is the one shown in Fig. 3d.

A very different picture emerges for the (6+1)ΛS, where the concept of a resonance ridge seizes to be applicable. As displayed in Fig. 6, in the vicinity of the resonance ridge of the 6LS P_F fluctuates through a multitude of local maxima and minima of different height due to additional interference contributions involving $|B\rangle$, and the projection of the global maxima in the (A_0, Δ_{ptp}, δ_{ptp})-subspace at fixed ω onto the (ω, A_0)-plane becomes irregular. This behavior is particularly pronounced for 4-trains, and finds its expression also in the population dynamics: the massively irregular pattern in Fig. 4c corresponds to the first maximum along the cut in Fig. 6b. Irregular elements are also manifest in the 8-trains in form of transient intruder state population, as *e.g.* in Fig. 4b and d, although below we will see that the regular elements still dominate and determine the behavior.

4.3. Phase recurrence and zero-order estimates

We now consider regular solutions obtained for methods A ($\omega = \omega_0^{IF}$) and B ($\omega = \omega_0^{IB}$) of Sec. 3.3, and relate them to the zero-order estimates given in Sec. 3. Characteristic features connected with the phase recurrence behavior are found in contour plots of target- and intruder state populations over the ($\Delta_{ptp}, \delta_{ptp}$)-plane. Fig. 7 and 8 show the results for 2-photon transitions by 4-trains in the (3+1)ΛS and the (3+1)LS, respectively, and Fig. 9 shows 8-train excitation of the 5-photon transition in the (6+1)LS. In all examples the sub-pulses are spectrally narrow enough to avoid final population of the anharmonically detuned rung states; hence all setups belong to *m*-regime I. The results are obtained for trains with optimized amplitudes A_0 The question whether the (ω, A_0)-pairs are thus points on a resonance ridge as in the background-free systems was already addressed in Section 4.2.

For $\omega = \omega_0^{\mathrm{IF}}$ (method A), P_{F} is accumulated at Δ_{ptp}-independent optimal values of δ_{ptp}, and population transfer to the target state is impeded only by the recurring contribution of the intruder. Caution with this statement is required in cases where the transition to the background state is dominant. Then the recurring contribution of the intruder may still imply that only those narrow ranges of Δ_{ptp} are available, where the intruder transition is *fully* quenched. In such a case it may be preferable to use method B, where at $\omega = \omega_0^{\mathrm{IB}}$ the *intruder state* has infinite recurrence time, and with δ_{ptp} taken appropriately, P_{B} is quenched by destructive interference for all values of Δ_{ptp}.

According to eq. (5), the *apparent* phase recurrence time for a transition with photonicity n is reduced by a factor $1/n$ due to the multiplicity of the recurrence pattern. Hence for a suitable value of δ_{ptp}, in method A n-photon population transfer to the target state proceeds optimally for values of Δ_{ptp} spaced by T_δ / n. Analogously, in method B maximum quenching of intruder state population occurs along straight lines in the $(\Delta_{\mathrm{ptp}}, \delta_{\mathrm{ptp}})$-plane spaced by T_δ / n', n' being the total photonicity of the $|\mathrm{I}\rangle \rightarrow |\mathrm{B}\rangle$ transition.

Zero-order estimates for π-trains driving selectively the $|\mathrm{I}\rangle \rightarrow |\mathrm{F}\rangle$ transition are obtained as crossings of constructive loci for P_{F} and destructive ones for P_{B}. These estimates are derived from eqs. (4). and (5); furthermore for each of the transitions a straight-line locus of constructive interference must emanate from the plot origin, which corresponds to the limit that all sub-pulses collapse into a single π-pulse. Figs. 4 to 6 bear out the expected phase-recurrence behavior: the computed probabilities closely match the estimates.

For the (3+1)ΛS and the (3+1)LS, the target-intruder energy mismatch is 3.8×10^{-6} au, corresponding to $T_\delta = 40$ ps. Hence in Figs. 7 and 8, for method A we observe periodicities in

P_B with respect to Δ_{ptp} of 40 ps for the (3+1)ΛS, with $n' = 1$, and of 13.33 ps for the (3+1)LS, with $n' = 3$. In method B, the periodicity of P_F is 20 ps in both systems ($n = 2$).

An appropriate zero-order estimate for π-train control in the (3+1)ΛS by method A is $\delta_{ptp} = \pi$ at $\Delta_{ptp} = 40$ ps. With this choice and an optimized value of A_0 we obtain $P_F = 0.984$. For all practical purposes, this zero-order choice produces the best specificity that can be can obtained with a 4-train in method A. A search for the global population maximum within method A gives only minimal improvement. Note however that the resulting train has an effective overall duration of 160 ps. Aiming at short train durations, a "pragmatic optimum" is $P_F = 0.981$ at $\delta_{ptp} = \pi$ for $\Delta_{ptp} = 5$ ps, with effectively *just* non-overlapping sub-pulses. Within methods A and B, selectivity approaching 100% can only be obtained by increasing the number of sub-pulses. Very selective PTC with 4-trains is obtained by detuning ω along the resonance ridge, as *e.g.* in the example in Fig. 4d.

For the (6+1)ΛS, the energy mismatch is 10^{-5} au, with $T_\delta = 15.2$ ps and effective recurrence times of 3.04 ps for the 5-photon $|I\rangle \rightarrow |F\rangle$ excitation. The contour plots in Fig. 9 show that the loci of maximum population transfer have the shape of steep, narrow ridges. The zero-order estimates seem to fall almost spot-on, yet due to the steepness of the ridges of maximum population, results obtained with zero-order train parameters are far off the 100% mark. Thus the zero-order estimate at (0.4π, $\Delta_{ptp} = 2.88$ ps) leads to $P_F = .796$. Upon re-optimization onto the slightly shifted true resonance locus at (0.411π, $\Delta_{ptp} = 3.07$ ps) we find $P_F = .994$. The persistence of partially irregular behavior contributes to these deviations from the zero-order estimates, but the narrowing of the features on the control landscapes accompanying the change from the (3+1)ΛS to the (6+1)ΛS also drastically reduces the robustness of control solutions. This narrowing has its roots both in multiplicity effects for

higher photonicities and in the higher number of sub-pulses required for high selectivity. On the other hand, due to the increased multiplicity a large array of possible zero-order solutions is at hand, naturally including also such of short train duration.

The similarities and the essential differences between methods A and B are evident in the one-dimensional cuts through the probability landscapes shown in Fig. 10. The Δ_{ptp}-dependence of P_{F} and P_{B} highlights the reciprocal role of target and intruder states in the two methods, while the phase portraits are closely alike and demonstrate that the underlying interference mechanisms are identical.

4.4. The number of sub-pulses

Whereas for irregular solutions the number of sub-pulses required for full control is hardly predictable, for the regular solutions there are clear trends in the *m*-dependence of the selectivity. For a systematic investigation of these effects we focus on the (3+1)ΛS and method A. In Fig. 11 we compare results for optimized 4-, 6-, 8- and 12-trains, which are analogous to the results of the background-free systems.[1] The plots indicate how the number of sub-pulses influences branch separation, and hence the achievable target population and residual intruder population. (P_{F} reaches 0.984 for 4-trains, 0.993 for 6-trains, 0.996 for 8-trains and 0.998 for 12-trains). They also show the trends in deviations from the zero-order solutions. With increasing *m*, the δ_{ptp} approach the zero-order values of eq. (4), and simultaneously the A_m decrease weakly.[1]

For the (3+1)LS, 12-trains fall already well into *m*-regime II, and the transition to this regime is accompanied by undesirable effects. Final rung state population becomes possible, and with their short phase-recurrence periods the rung states dominate the excitation pattern. In the (3+1)ΛS driven at $\omega = \omega_0^{\mathrm{IF}}$, massive rung state population recurs with $T_\delta = 1.22$ ps, and it is

tedious to locate a parameter set where both the intruder and the rung state are fully suppressed *and* the total train duration remains short. For more extended systems, these problems are further amplified by recurring contributions from several rung states with different values of T_δ, and a further reduction of the apparent recurrence times due to the higher multiplicities. This puts heavy demands on finding and keeping a suitable value of Δ_{ptp}, so that a practical implementation may be difficult.

4.5. Pulse train control and the mechanisms of resonance leaking

Close inspection of the contour plots in Sec. 4.3 provides more clues about the nature of the leaking processes. In the (3+1)ΛS the intruder transition is seen to be dormant over extended stretches of parameter space, and is revived only under conditions for which target population is also present. The field driving the 2-photon target transition is too weak to directly excite the $|\mathrm{I}\rangle \rightarrow |\mathrm{B}\rangle$ process, which involves 3 photons. Leaking occurs through the one-photon $|\mathrm{F}\rangle \rightarrow |\mathrm{B}\rangle$ transition, which follows target state excitation in a sequential two-step process. Hence intruder population appears together with target population where permitted by the phase relations, and is absent if the target transition is suppressed, and the peaks in P_B are aligned with P_F and do not follow the direction given by the zero-order estimates.

In contrast, in the (6+1)ΛS resonance leaking is an autonomous process using the target as intermediate ladder state in a (5-1)-photon transition, which occurs in parallel with the 5-photon target transition. In the contour plots the maxima of both P_F and P_B are ridge-shaped and aligned along the respective zero-order estimates. This indicates that except for the ptp phase shift both transitions are driven efficiently and independently by the same pulse train. Analysis of adiabatic Floquet states has led to similar conclusions about the existence of different mechanisms of resonance leaking.[13]

Our considerations support the interpretation that in the irregular solutions found for the (6+1)ΛS - but not for the (3+1)ΛS - the characteristic PTC mechanism based on phase matching and phase recurrence is more or less strongly augmented by two-pathway interferences of coherent-control type.[19]

5. PHASE-SENSITIVE LEVEL SWITCHING WITH PULSE TRAINS

The last statement of the previous section suggests an alternative application of PTC. According to eq. (4), processes of different photonicity have different optimal (constructive) ptp phase shifts. These properties render pulse trains a tool for phase-sensitive level switching. Indeed, as is evident from Fig. 10, tuning δ_{ptp} in the (6+1)ΛS causes a switch of population between target state (99 %) and intruder state (76 %). Both switch positions correspond to closely state-selective excitation: even if the population does not reach 100%, the remaining fraction always resides largely in the initial state. By readjustment of the train parameters for improved switching rather than for intruder control, P_{B} can be increased to 90%, with the target state population still 99%. The switch characteristics can also be made symmetric. Figs.12 and 13 illustrate a device operating with populations of ≈97% for both switch positions. Furthermore the device is neutral for ptp phase shifts in between the switch positions, where the system to a large extent remains in the initial state.

We note that a phase-driven switch between two available final states was also found for population transfer in dipolar systems by an mp variant of STIRAP (stimulated Raman-adiabatic passage).[22]

6. SUMMARY AND CONCLUSIONS

In this paper we have introduced and discussed PTC of branching and competing mp transitions. Our control strategies rely on phase-matching and phase-recurrence properties of resonant population transfer by pulse trains and the different response of these properties for processes with different photonicities and possibly different, but near-degenerate transition frequencies.[1] Based on the choice of the central frequency of the pulse trains, three specific control strategies are suggested, which are capable of eliminating an undesirable branch and promoting a desirable one in branching and competing population transfer processes, and thus can steer the system specifically to a selected target state. As an example of PTC of competing processes, elimination of background- (intruder-) state population in resonance leaking has been demonstrated on the basis of simulations for *N*-level model systems. This situation involves processes with different photonicities and near-degenerate transition frequencies.

We observe what we call regular and irregular solutions to the control problem. The regular mechanism is based on phase-matching and phase-recurrence and is identical to the one governing mp pulse train excitation in unperturbed ladder progressions.[1,5-9] Control strategies using zero-order resonance frequencies can be applied and investigated systematically starting out from zero-order estimates. We find that this way a leaking two-photon transition can be controlled with ease, and the trains and the ensuing population dynamics strongly resemble the trains effecting population transfer in the background-free reference system. The option to freely tune the frequency over a range approximately given by the resonance ridges of the background-free systems greatly assists the separation of the competing processes and helps keeping the number of sub-pulses small.

In more complex systems and for transitions of higher photonicity fully selective regular control solutions based on phase matching and phase recurrence may require many sub-pulses to an extent becoming awkward in practical implementation. In this case optimal control can

produce more efficient irregular solutions, *i.e.* specific solutions that have no direct counterpart in the background-free system, but tend to retain the qualitative features of the simple control schemes. This involves optimization on a rugged control landscape with multiple local maxima, rendering an *a priori* treatment of PTC based on zero-order estimates difficult or unlikely.

In alternative setup, the control properties of π-trains can be utilized for a phase-sensitive level switch, such that by varying only the ptp-phase shift, population is switched between the final states of the branching processes. In the present investigation we have demonstrated such a population switch between target and intruder state of a leaking resonant mp transition; however the concept can be extended to other situations involving population branching.

Work in progress in this laboratory indicates that PTC is applicable *e.g.* in the control of population branching involving *strongly* coupled intruder states. In a different connection, we draw attention to the control fields obtained by Laarman *et al*. [23] in a closed-loop self learning pulse shaping experiment, in which the cleavage yield of a pre-selected backbone bond in an amino acid complex is optimized. The genetic algorithm steering this optimization produces a 3-train with a ptp-phase shift of π. In the light of the discussions in ref. 1 and the present paper one could speculate that the algorithm found a PTC strategy promoting two-photon (or other even mp) processes and blocking one-photon (or other uneven mp) transitions.

ACKNOWLEDGMENTS

This work was supported by the Austrian Science Fund within the framework of the Special Research Program F016 "ADLIS". ME expresses his gratitude for a visiting grant from the Faculty of Chemistry of the University of Vienna.

REFERENCES

[1] M. Seidl, C. Uiberacker, and W. Jakubetz, Chem. Phys. **349**, 296 (2008).

[2] L. Allen and J. H. Eberly, Optical Resonance and Two Level Atoms, Wiley, New York, 1975; M. Grifoni and P. Hänggi, Phys. Rep. **304**, 229 (1998).

3 I.I. Rabi, Phys. Rev. **51**, 652 (1937).

[4] S. Chelkowski, A. D. Bandrauk, and P. B. Corkum, Phys. Rev. Lett. 65 (1990) 2355; M. Holthaus and B. Just, Phys. Rev. A **49**, 1950 (1994).

[5] N.V. Vitanov and P.L. Knight, Phys. Rev. A **52**, 2245 (1995).

[6] S. Besnainou, J.-C. Diels, and J. Stone, J. Chem. Phys. **81**, 143 (1984); J.-C. Diels and S. Besnaiou, J. Chem. Phys. **85**, 6347 (1986); R.J. Temkin, J. Opt. Soc. Am. B **10**, 830 (1993).

[7] A.M. Weiner, D.E. Leaird, G.P. Wiederrecht, and K.A. Nelson, Science **247**, 317 (1990); A.M. Weiner, D.E. Leaird, G.P. Wiederrecht, and K.A. Nelson, J. Opt. Soc. Am. B **8**, 1264 (1991).

[8] D. Felinto, C.A.C. Bosco, L.H. Acioli, and S.S. Vianna, Phys. Rev. A **64**, 063413 (2001); D. Felinto, C.A.C. Bosco, L.H. Acioli, and S.S. Vianna, Opt. Commun. **215**, 69 (2003); D. Felinto, L.H. Acioli, and S.S. Vianna, Phys. Rev. A **70**, 043403 (2004).

[9] W. Yang, Sh. Gong, R. Li, and Zh. Xu, Phys. Rev. A **74**, 013407 (2006).

[10] A. Pe'er, E.A. Shapiro, M.C. Stowe, M. Shapiro, and J. Ye, Phys. Rev. Lett. **98**, 113004 (2007); E. A.Shapiro, V. Milner, C.Menzel-Jones, and M. Shapiro, Phys. Rev. Lett. **99**, 033002; S. Zhdanovich, E. A. Shapiro, M. Shapiro, J. W. Hepburn, and V. Milner, Phys. Rev. Lett. **100**, 103004.

[11] J. Hauer, T. Buckup, and M. Motzkus, J. Chem. Phys. **125**, 061101 (2006); T. Buckup, J. Hauer, C. Serrat and M. Motzkus, J. Phys. B: At. Mol. Opt. Phys. **41**, 074024 (2008).

[12] T. Uzer and W. H. Miller, Phys. Rep. **199**, 73 (1991).

[13] W. Jakubetz and B.-L. Lan, J. Chem. Phys. **117**, 7968 (2002).

[14] B.-L. Lan, I. Vrábel, and W. Jakubetz, J. Chem. Phys. **121**, 10401 (2004); M. Etinski, C. Uiberacker, and W. Jakubetz, J. Chem. Phys. **124**, 124110 (2006).

[15] J.M. Bowman, B. Gazdy, J.A. Bentley, T.J. Lee, and C.E. Dateo, J. Chem. Phys. **99**, 308 (1993).

[16] F. Bloch, A. Siegert, Phys. Rev. **57**, 522 (1940); P.K. Aravind, J.O. Hirschfelder, J. Phys. Chem. **88**, 4788 (1984). Note we use the term "Bloch-Siegert shift" for any field-induced resonance shift of pulse-driven transitions in *N*-level systems.

[17] W. Jakubetz and B.-L. Lan, Chem. Phys. **217**, 375 (1997); P. Botschwina, M. Horn, M. Matuschewski, E. Schick, and P. Sebald, J. Mol. Struct. THEOCHEM **400**, 119 (1997).

[18] H. Rabitz, Adv. Chem. Phys. **101**, 315 (1997); A. Peirce, M. Dahleh, and H. Rabitz, Phys. Rev. A **37**, 4950 (1988), S. Shi and H. Rabitz, J. Chem. Phys. **92**, 2927 (1990).

[19] W. Zhu, J. Botina, and H. Rabitz, J. Chem. Phys. 108 (1998) 1953; W. Zhu and H. Rabitz, J. Chem. Phys. **119,** 3619 (2003).

[20] A. Assion, T. Baumert, T. Bergt, B. Brixner, B. Kiefer, M. Seyfried, M. Strehle, and G. Gerber, Science **282**, 919 (1998); G. Gerber, T. Brixner, M. Wollenhaupt, and T. Baumert, in *Femtosecond Laser Spectroscopy*, edited by P. Hannaford, (Kluwer, Dordrecht, 2004), p. 229.

[21] M. Shapiro and P. Brumer, Advan. At. Mol. Opt. Phys. **42**, 287 (2000); P. Brumer and M. Shapiro, Chem. Phys. Lett. **126**, 541 (1986).

[22] C. A. Marx and W. Jakubetz, J. Chem. Phys. **125**, 234103 (2006).

[23] T. Laarmann, I. Shchatsinin, P. Singh, N. Zhavoronkov, C. P. Schulz, and I. V. Hertel, J. Phys. B: At. Mol. Opt. Phys. **41**, 074005 (2008).

Tables

TABLE I. Zero-order transition frequencies in the model systems

	(3+1)ΛS (3+1)LS [a]	(6+1)ΛS
ω_0^{IF} [b]	.004 375	.004 750
ω_0^{FB} [c]	.004 379	.004 790

[a] Same values for simple and embedded systems

[b] (k-1)-photon initial state-to-target state zero-order transition frequency (circular frequency)in a.u. in the (k+1)LS

[c] One-photon target state-to-background state zero-order transition frequency (circular frequency) in a.u.

TABLE II. Properties of 8 ps gaussian π-pulses in the model systems [a]

	(3+1)ΛS	(3+1)LS	(6+1)ΛS
ω_{r} [a]	0.00437504	0.00437491	0.00479162
A_{r} [b]	0.000295	0.000295	0.003127
P_{B} [c]	34.2	34.2	83.5

[a] Resonance frequency (circular frequency) in a.u.

[b] Peak field strength in a.u.

[c] Background (intruder) state population in % (amount of leaking)

Figure Captions

Fig.1: Level schemes of the model systems. A state $|\mathrm{B}\rangle$ is weakly coupled to a ladder state $|\mathrm{F}\rangle$ of a strongly coupled anharmonic progression. Left: the [embedded] (3+1)-level system in Λ-configuration denoted (3+1)ΛS. Middle: the [embedded] (3+1)-level system in ladder-configuration denoted (3+1)LS. Right: The (6+1)-level system in Λ-configuration denoted (6+1)ΛS. Resonant multiphoton transitions from the initial state $|\mathrm{I}\rangle$ to the final (target) state $|\mathrm{F}\rangle$ indicated by arrows strongly leak to the background (intruder) state $|\mathrm{B}\rangle$.

Fig. 2: Envelope functions of gaussian pulses and pulse trains. (a): A gaussian pulse envelope (online red) with pulse width (fwhh) Tp = 8 ps, and a 6-train (of $\pi/6$ pulses) with sub-pulse width $T_\mathrm{p}/6$ and the pulse-to-pulse time delay Δ_ptp adjusted for equal effective pulse and train durations. (b) The gaussian pulse compared with a 6-train with non-overlapping sub-pulses of width T_p (dashed line) and the 6-train of panel a with Δ_ptp increased to span the same effective train duration (full line). All shapes are to scale for resonant two-photon transitions in the (3+1)ΛS.

Fig. 3: PTC solutions for intruder suppression in the two-photon transition for the (3+1)ΛS. Top row: the envelope functions (field strength in arbitrary units, but to scale for the four fields a-d). Bottom row: the corresponding population dynamics. Bold lines (online blue): target population P_F, thin lines (online red): intruder population P_B, dashed gray lines: initial state population P_I. (a) The leaking resonant transition induced by the gaussian reference pulse. (b) 6-train solution with $\omega = \omega_0^{\mathrm{IF}}$ (method A). (c) 6-train solution with $\omega = \omega_0^{\mathrm{IB}}$ (method B) for a 5π-train of $5\pi/6$ sub-pulses. (d) 4-train solution at strongly detuned frequency (point marked "A" in Fig. 5).

Fig. 4: PTC solutions as in Fig 3, but for the five-photon transition in the (6+1)ΛS. (a) The leaking resonant transition with the gaussian reference pulse. (b) 8-train solution with $\omega = \omega_0^{\mathrm{IF}}$ (method A with irregular contributions; point marked "B" in Fig. 6). (c) 4-train solution with $\omega = \omega_0^{\mathrm{IF}}$ (irregular solution, point marked "C" in Fig. 6). (d) 4-train solution at detuned frequency (point marked "D" in Fig. 6).

Fig. 5: Frequency dependence of PTC solutions in the (3+1)ΛS. (a) Projections of the parameters of the 4-train giving maximum target population at fixed ω onto the (ω, A_0)-plane, shown as filled circles, are compared with the resonance ridge of the 3LS (continuous line). Lower and upper parts of the resonance ridge and the PTC solutions in the vicinity correspond respectively to π-trains and 7π-trains. Line segments marked "b" and "c" refer to panels b and c. (b) Target population along line segment "b" of panel (a), corresponding to $\omega = \omega_0^{\mathrm{IF}}$. Full line: 3LS; symbols: (3+1)ΛS. (c) T_{p} along line segment "c" of panel a. Plot details as in panel a. Population dynamics for train indicated by "A" are shown in Fig. 3d.

Fig. 6: Frequency dependence of PTC solutions in the (6+1)ΛS. (a) Projections as in Fig. 5a, of the parameters for 4-trains (full circles) and 8-trains (open squares), and corresponding resonance ridges for the 6LS (dashed line: 4-trains; full line: 8-trains). Only the π-branches of the resonance ridges are included. (b) Target populations along the cut $\omega = \omega_0^{\mathrm{IF}}$ for 4-trains. Full line: 6LS; symbols: (6+1)ΛS. (c): As panel (b), but for 8-trains. Population dynamics for trains indicated by "B", "C" and "D" are shown in Fig. 4b-d.

Fig. 7: Contour plots of final populations P_F and P_B over the $(\Delta_{ptp}, \delta_{ptp})$-plane for two-photon excitation with 4-trains in the (3+1)ΛS. Results obtained for $\omega = \omega_0^{IF}$ or ω_0^{IB} as indicated; train amplitude A_0 fixed at optimal value within parameter subspace orthogonal to ω. Various zero-order estimates are indicated by straight lines: Bold full lines (online cyan): constructive for target state, dashed lines (online red): constructive for intruder state, thin full lines (online green): destructive for intruder state. In the top row panels, intersection points of *full* lines indicate zero-order estimates for full target population.

Fig. 8: Contour plots as in Fig. 7, but for 4-trains in the (3+1)LS.

Fig. 9: Contour plots as in Fig. 7, but for 8-trains in the (6+1)ΛS.

Fig. 10: Comparison of phase matching and phase recurrence properties in method A, $\omega = \omega_0^{IF}$ (top row), and method B, $\omega = \omega_0^{IB}$ (bottom row). Results are for 8-trains in the (6+1)ΛS with individually optimized train amplitudes A_0. Bold lines (online blue): target population P_F; thin lines (online red): intruder population P_B. Panels (a), (b): Δ_{ptp}-dependence of P_F and P_B with δ_{ptp} fixed as indicated by arrows in panels (c) and (d). Panels (c), (d): Phase portraits (δ_{ptp}-dependence of P_F and P_B) with Δ_{ptp} fixed as indicated by arrows in panels (a) and (b).

Fig. 11: Dependence of pulse train properties on the number of sub-pulses for method A, $\omega = \omega_0^{\mathrm{IF}}$. Results are for the (3+1)ΛS. Blue lines: target population P_{F}; red lines: intruder population P_{B}; dark green lines: rung population P_2; dashed gray lines: initial state population P_{I} (where shown). Left column: Δ_{ptp}-dependence of P_{F}, P_{B} and $P_{2.}$ Middle column: Phase portraits. Right column: Population dynamics for optimized PTC fields. Rows a to d in turn show 4-, 6-, 8- and 12-trains. In this setup, 8-trains fall just and 12-trains fall well into *m*-regime II.

Fig. 12: Population response of a phase sensitive level switch operating between levels $\left|\mathrm{F}\right\rangle$ and $\left|\mathrm{B}\right\rangle$ of the (6+1)ΛS. Parameters of an 8-train tuned to $\omega = \omega_0^{\mathrm{IF}}$ are adjusted to produce the best symmetric population switch between switch positions marked “B” and “F”. Bold line (online blue): P_{F}; thin line (online red): P_{B}; dashed gray line: P_{I}.

Fig. 13: Envelope functions (top panels) and population dynamics (bottom panels) for the two switch positions “F” and “B” of the level switch of Fig. 12. Plot details are also as in Fig. 12.

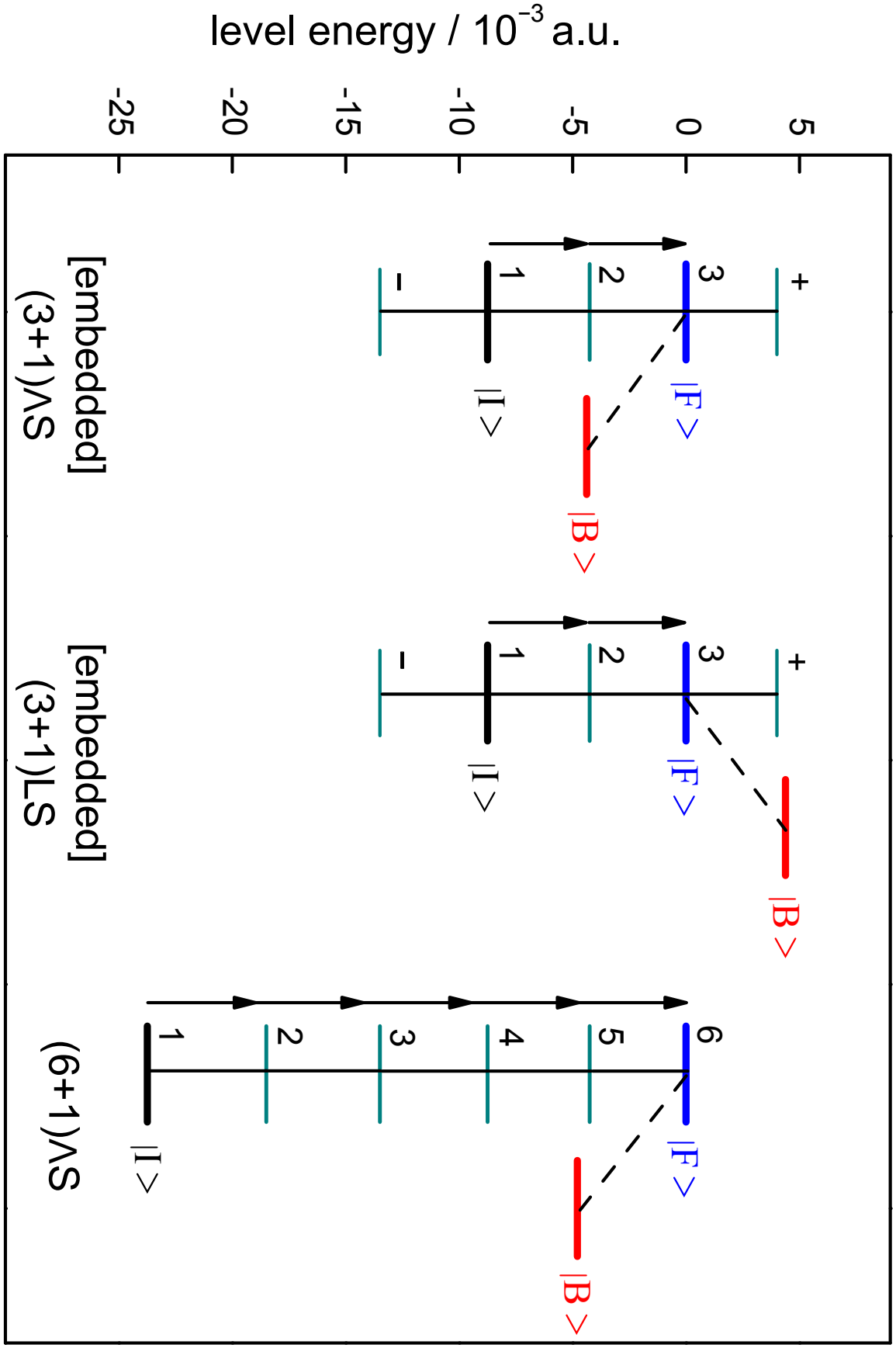
level energy / 10^-3 a.u.
-25
-20
-15
-10
-5
0
5
[embedded]
(3+1)ΛS
[embedded]
(3+1)LS
(6+1)ΛS
1
2
3
4
5
6
+
-
|I>
|F>
|B>

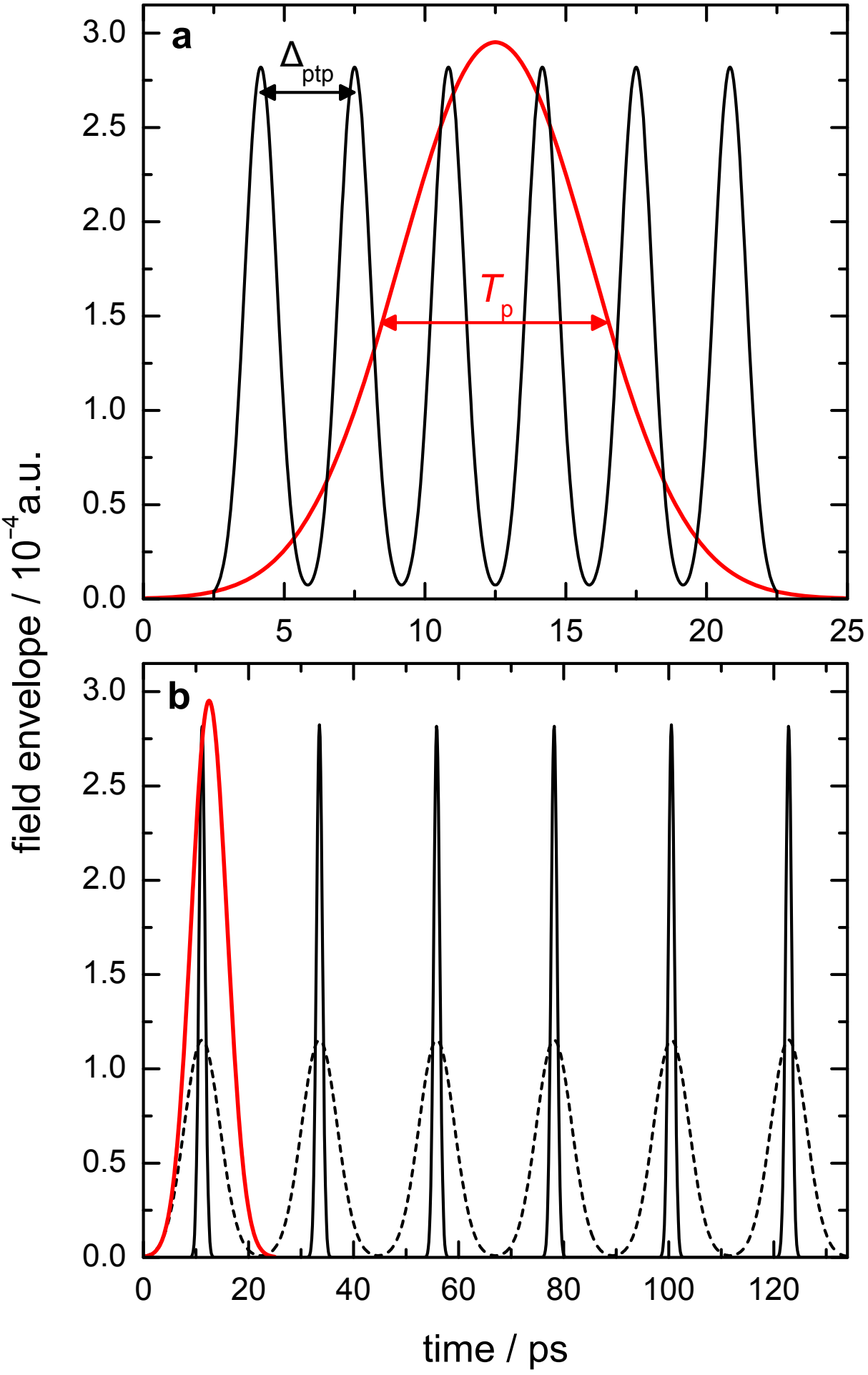
a
b
Δ_{ptp}
T_p
field envelope / 10^{-4} a.u.
time / ps
0.0
0.5
1.0
1.5
2.0
2.5
3.0
0
5
10
15
20
25
0
20
40
60
80
100
120

FIG. 3

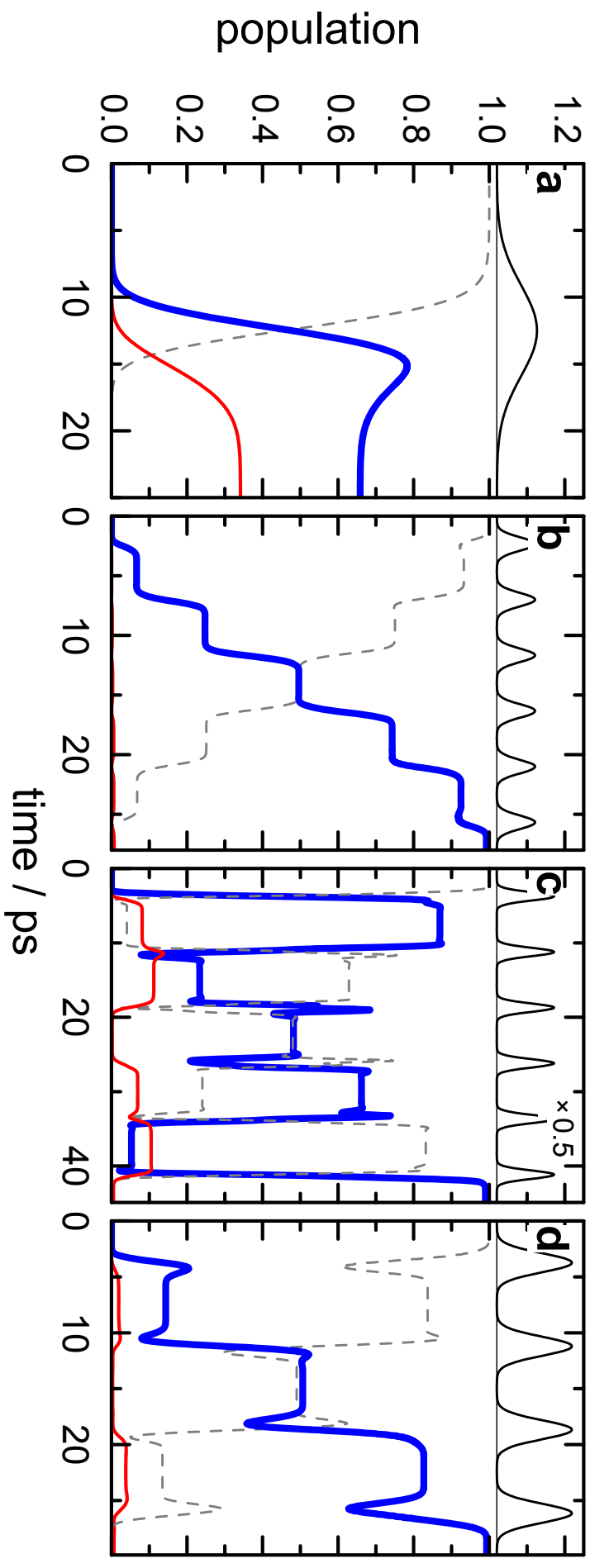
population
0.0
0.2
0.4
0.6
0.8
1.0
1.2
a
b
c
d
×0.5
0
10
20
0
10
20
0
20
40
0
10
20
time / ps

FIG. 4

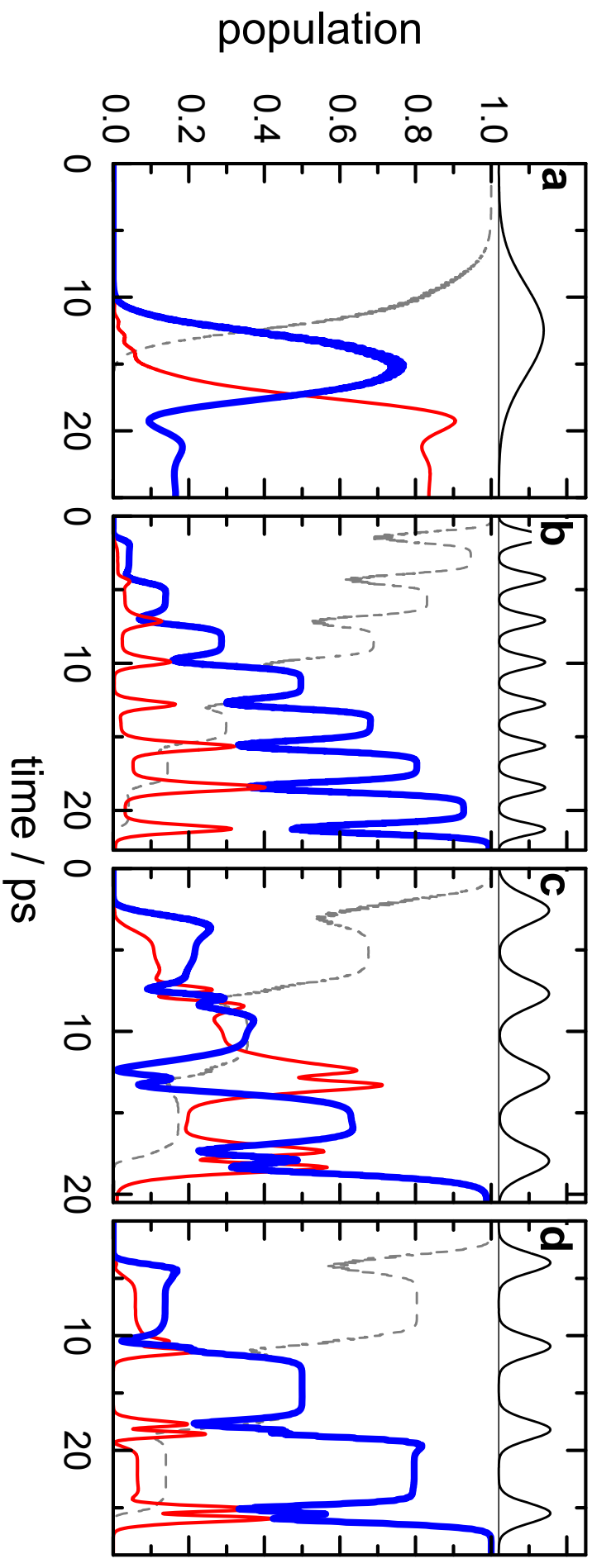

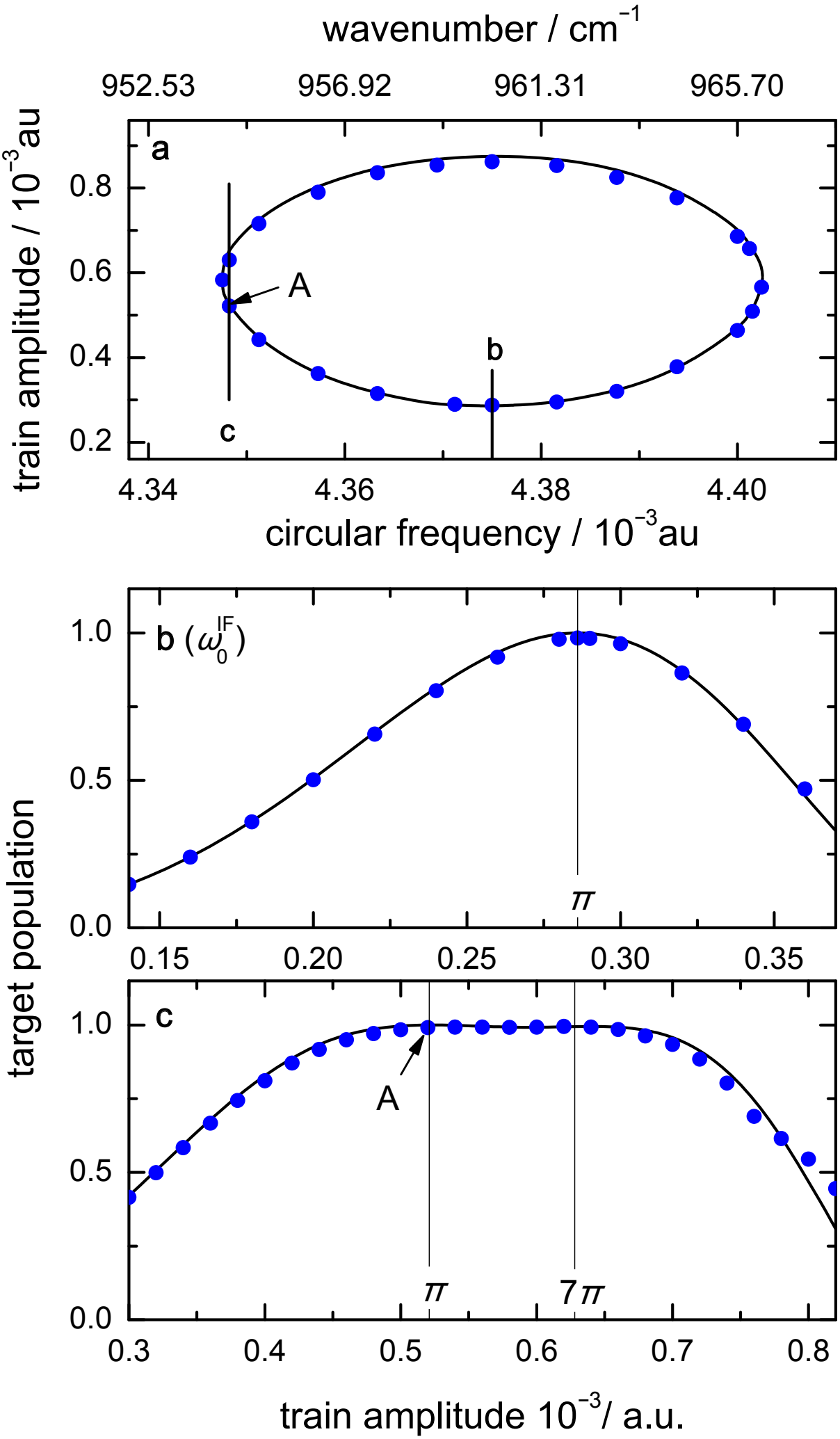
wavenumber / cm^{-1}
952.53
956.92
961.31
965.70
a
train amplitude / 10^{-3}au
0.8
0.6
0.4
0.2
A
b
c
4.34
4.36
4.38
4.40
circular frequency / 10^{-3}au
b (ω_0^{IF})
1.0
0.5
0.0
π
0.15
0.20
0.25
0.30
0.35
target population
c
1.0
0.5
0.0
A
π
7π
0.3
0.4
0.5
0.6
0.7
0.8
train amplitude 10^{-3}/ a.u.

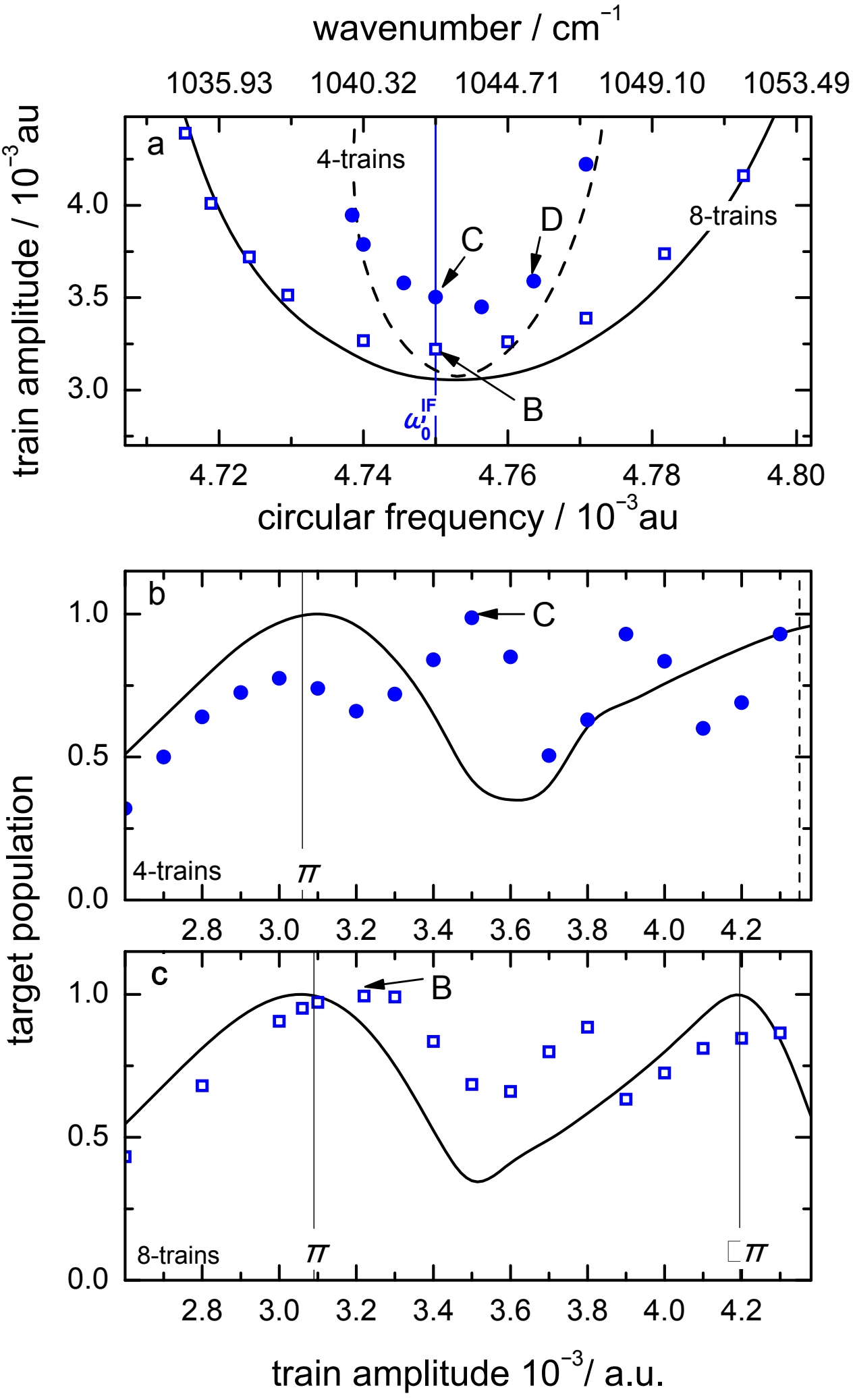
wavenumber / cm^{-1}
1035.93
1040.32
1044.71
1049.10
1053.49
a
4-trains
8-trains
C
D
B
ω_0^{IF}
train amplitude / 10^{-3}au
4.0
3.5
3.0
4.72
4.74
4.76
4.78
4.80
circular frequency / 10^{-3}au
b
C
4-trains
π
1.0
0.5
0.0
2.8
3.0
3.2
3.4
3.6
3.8
4.0
4.2
c
B
8-trains
π
π
target population
train amplitude 10^{-3}/ a.u.

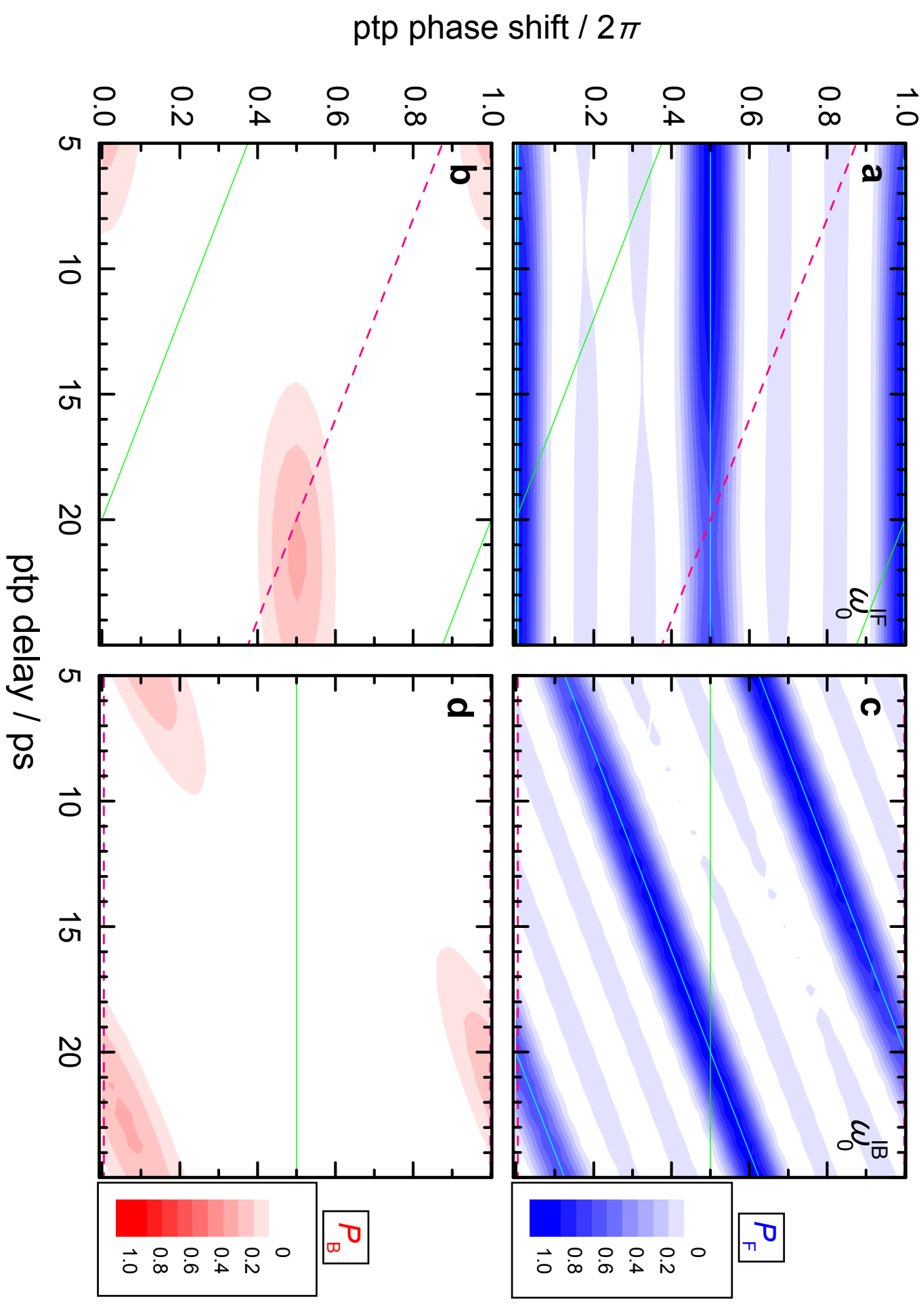
ptp phase shift / 2π
ptp delay / ps
a
b
c
d
ω_0^{IF}
ω_0^{IB}
P_F
P_B
0.0
0.2
0.4
0.6
0.8
1.0
5
10
15
20

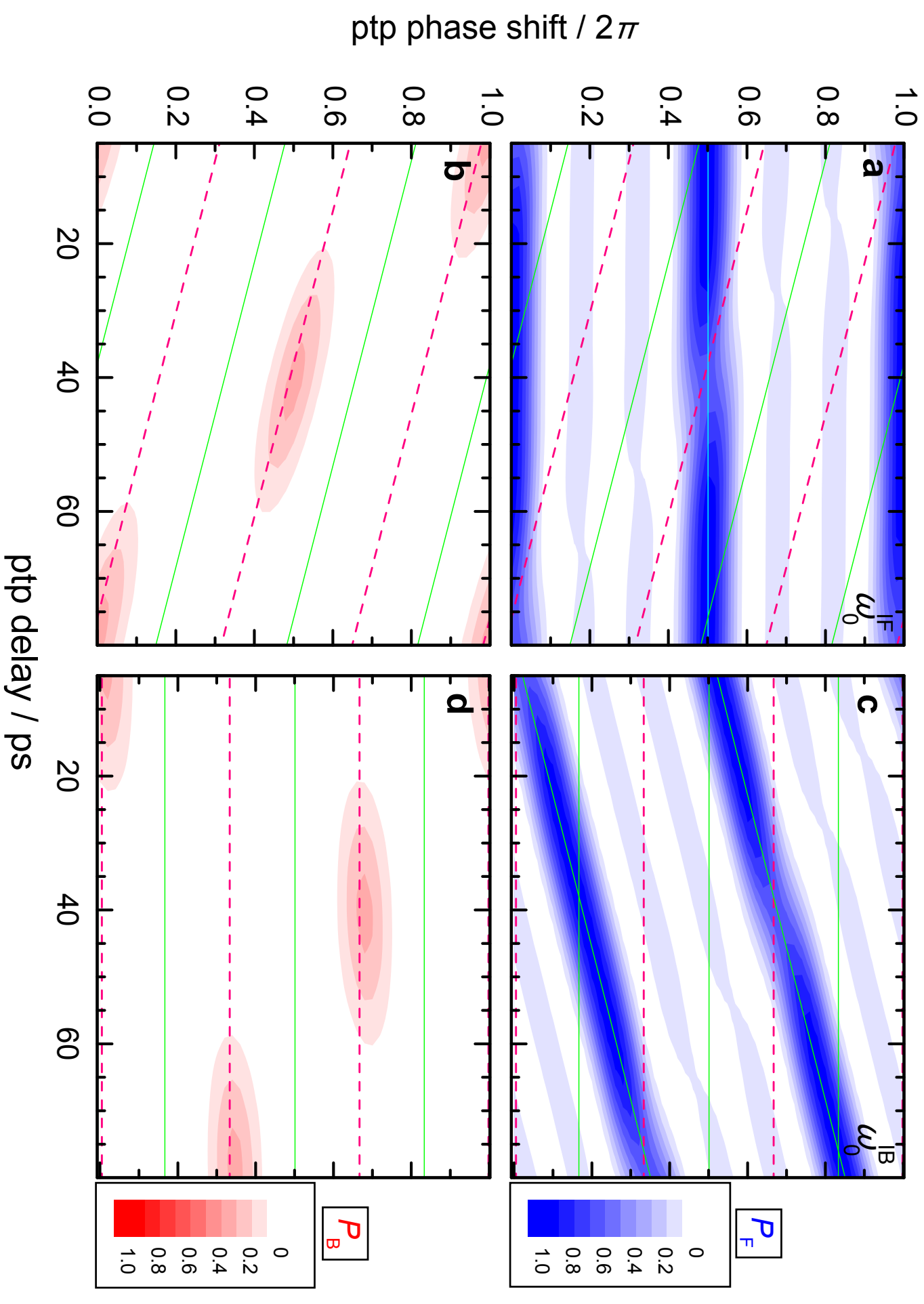
ptp phase shift / 2π
ptp delay / ps
a
b
c
d
ω_0^{IF}
ω_0^{IB}
P_F
P_B
0.0
0.2
0.4
0.6
0.8
1.0
20
40
60

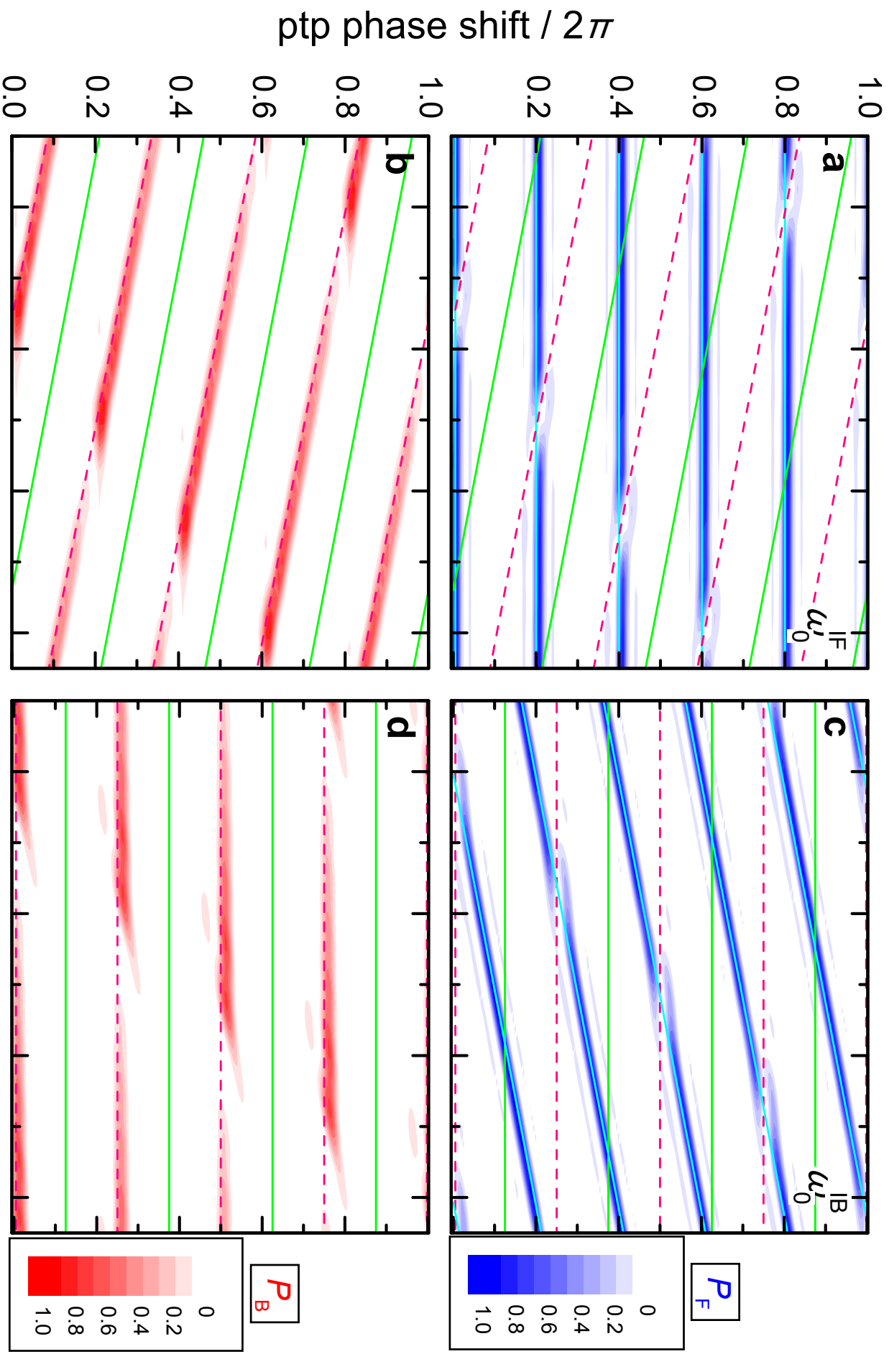
ptp phase shift / 2π
ppt time delay / ps
a
b
c
d
ω_0^{IF}
ω_0^{IB}
P_F
P_B
0.0
0.2
0.4
0.6
0.8
1.0
3
4
5
6

FIG. 10

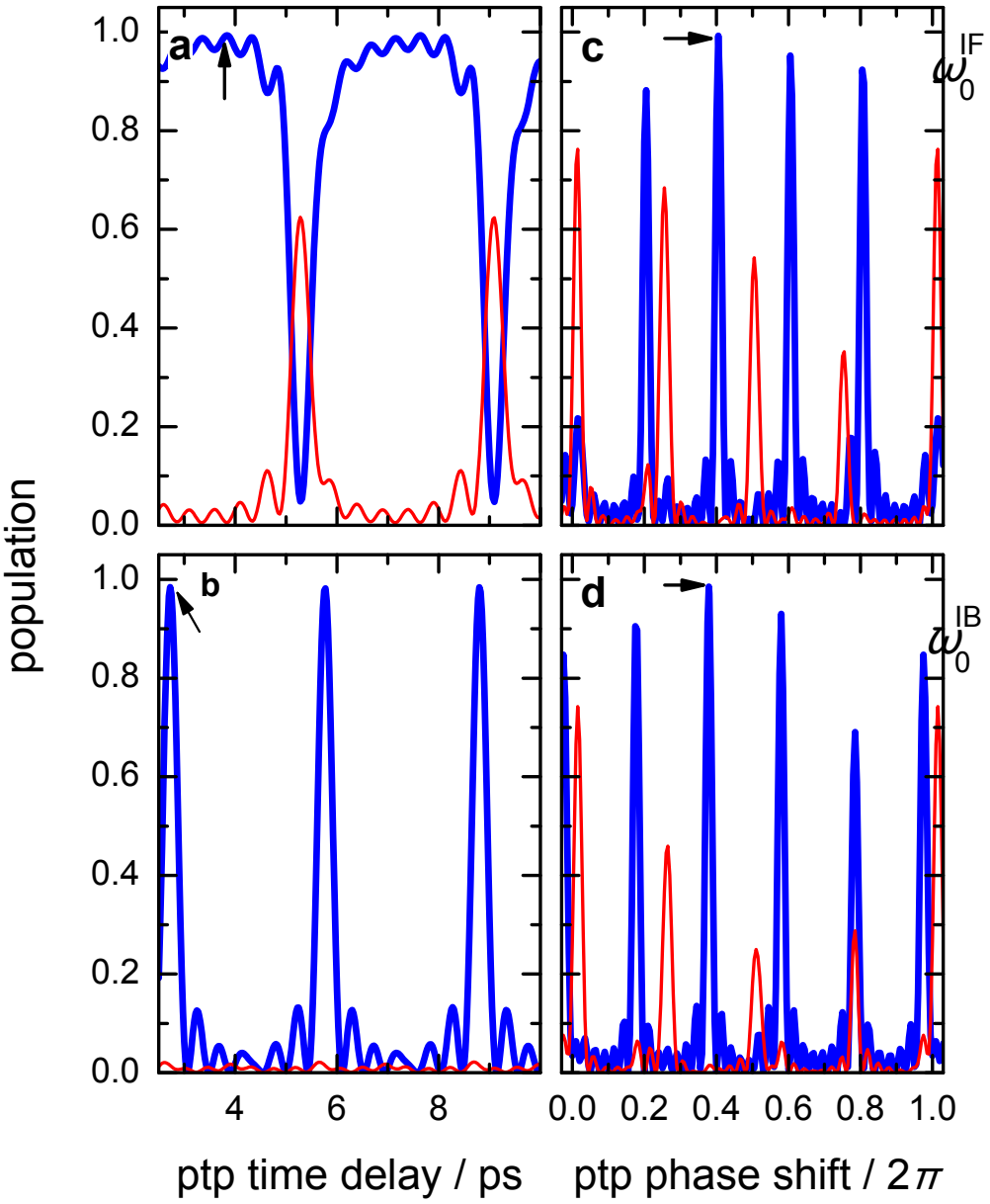
a
b
c
d
IF
IB
ω_0
population
1.0
0.8
0.6
0.4
0.2
0.0
4
6
8
0.0
0.2
0.4
0.6
0.8
1.0
ptp time delay / ps
ptp phase shift / 2π

FIG. 11

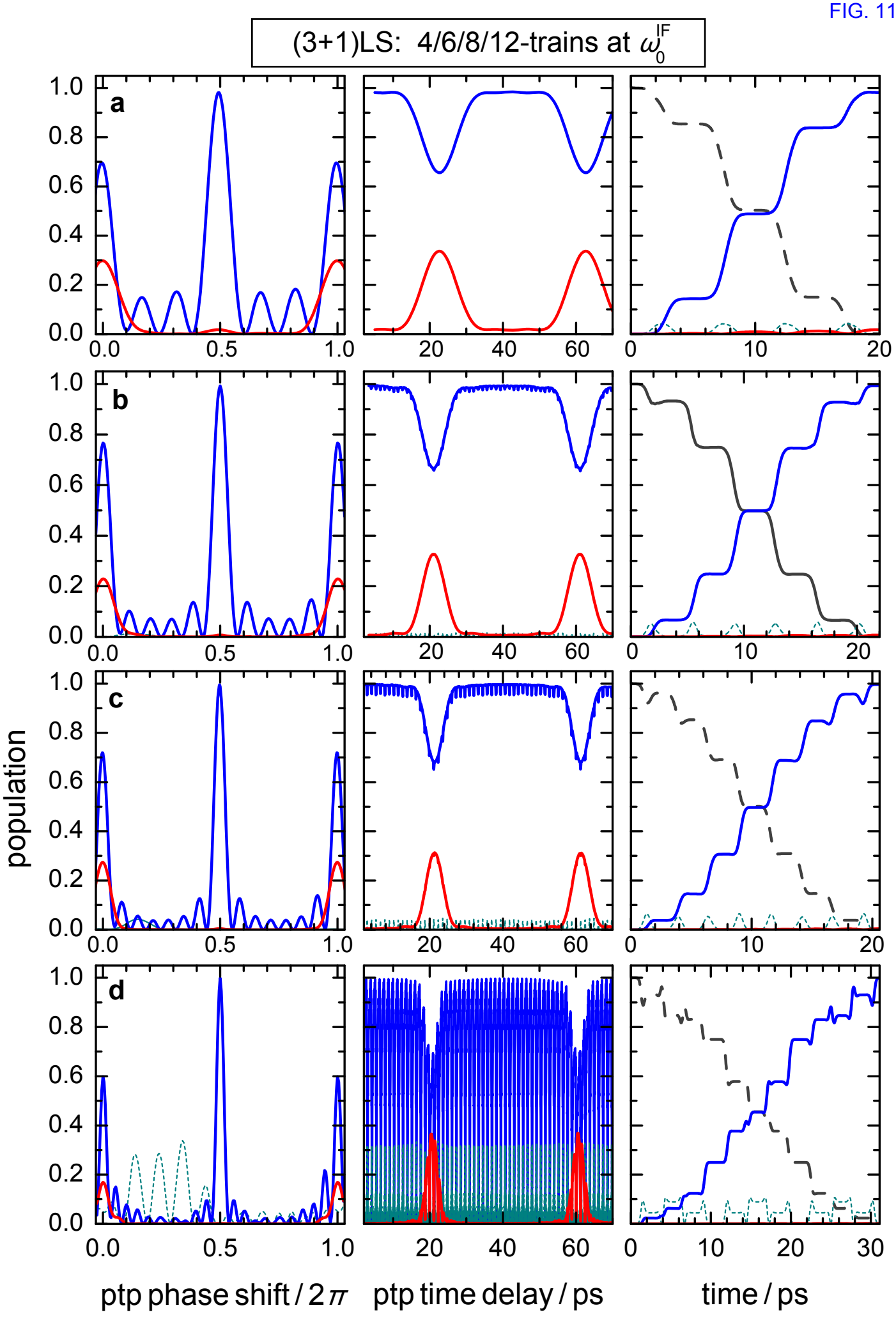
(3+1)LS: 4/6/8/12-trains at ω_0^{IF}
a
b
c
d
population
ptp phase shift / 2π
ptp time delay / ps
time / ps

FIG. 12

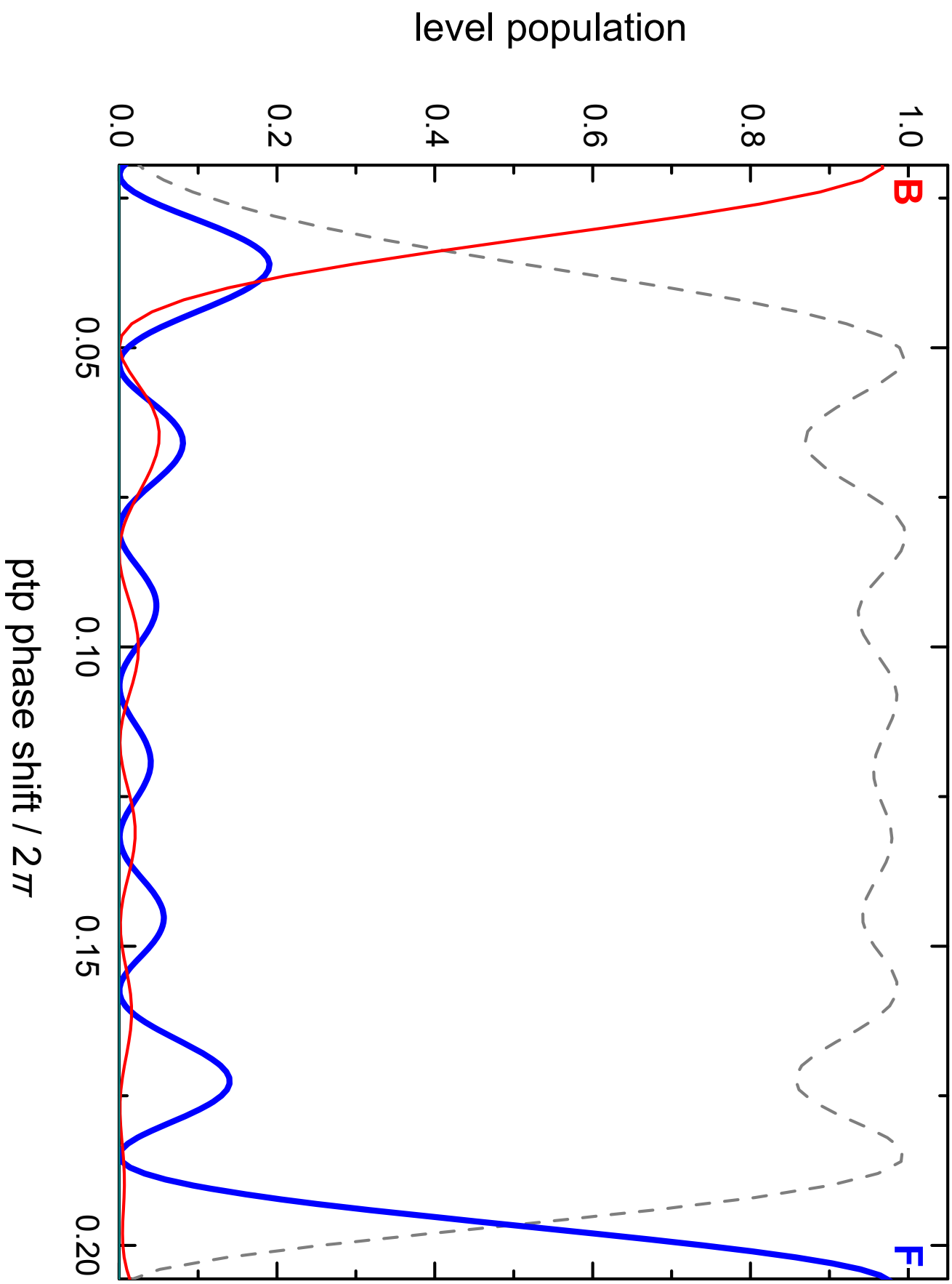
level population
0.0
0.2
0.4
0.6
0.8
1.0
B
F
0.05
0.10
0.15
0.20
ptp phase shift / 2π

FIG. 13

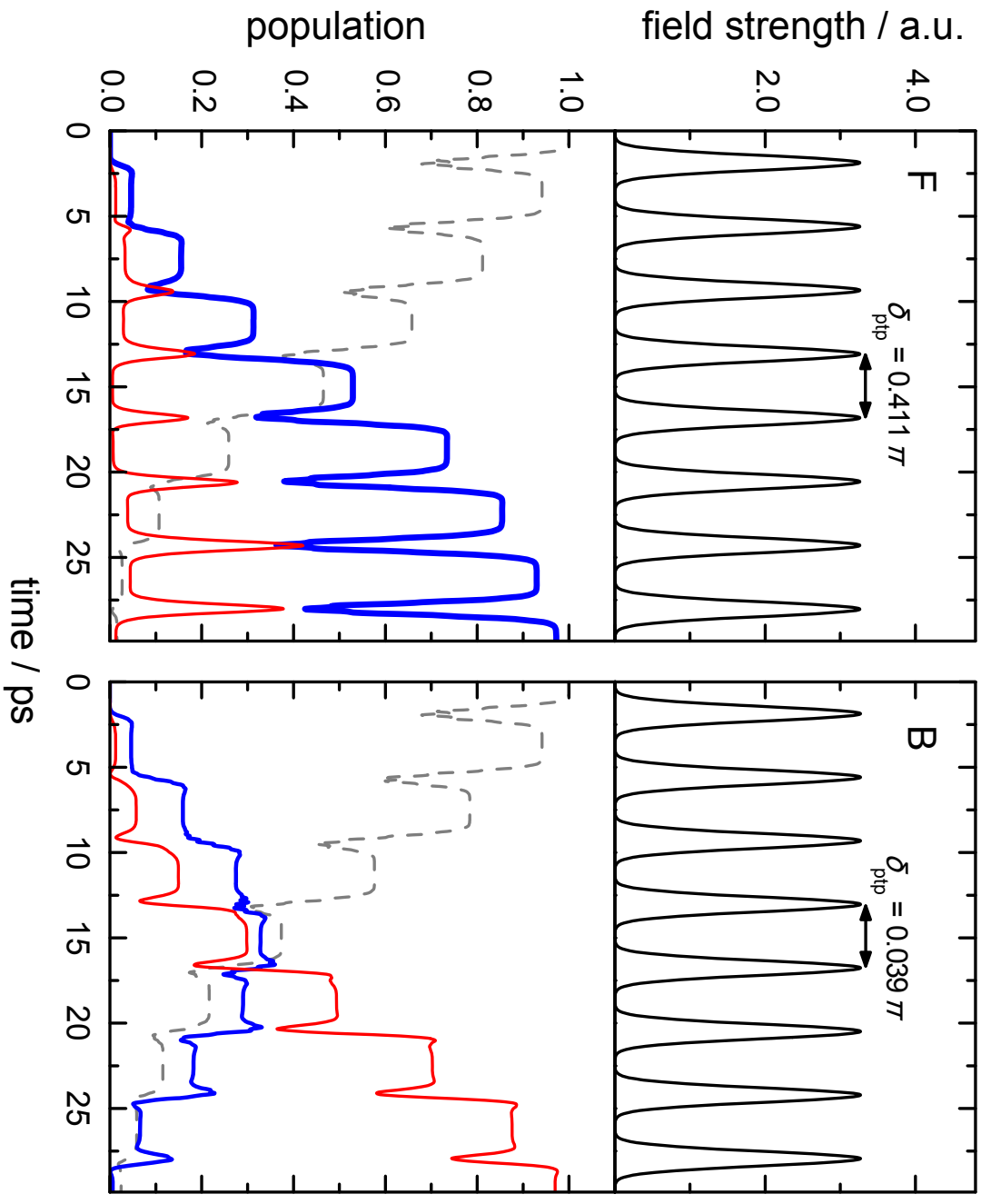
field strength / a.u.
population
time / ps
F
B
δ_{ptp} = 0.411 π
δ_{ptp} = 0.039 π
4.0
2.0
1.0
0.8
0.6
0.4
0.2
0.0
0
5
10
15
20
25